Thermally Driven Mesoscale Chemomechanical Interplay in $Li_{0.5}Ni_{0.6}Mn_{0.2}Co_{0.2}O_2$ Cathode Materials

Chenxi Wei, ‡[ac] Yan Zhang, ‡[bc] Sang-Jun Lee, ‡[c] Linqin Mu,[d] Jin Liu,[e] Chenxu Wang,[e] Yang Yang,[f] Marca Doeff,[g] Piero Pianetta,[c] Dennis Nordlund,[c] Xi-Wen Du,[b] Yangchao Tian,*[a] Kejie Zhao,[h] Jun-Sik Lee,[c] Feng Lin,*[d] Yijin Liu, *[c]

While the Li ion batteries are intended to be operated within a mild temperature window, their structural and chemical complexity could lead to unanticipated local electrochemical events that could cause extreme temperature spikes, which, in turn, could trigger more undesired and sophisticated reactions in the system. Visualizing and understanding the response of battery electrode materials to the thermal abuse conditions could potentially offer a knowledge basis for prevention and mitigation of the safety hazards. Here we show a comprehensive investigation of the thermally driven chemomechanical interplay in a $Li_{0.5}Ni_{0.6}Mn_{0.2}Co_{0.2}O_2$ (charged NMC622) cathode material. We report that, at the early stage of the thermal abuse, the oxygen release and internal Li migration occur concurrently, and are accompanied by the mechanical disintegration at the mesoscale. At the later stage, Li protrusions are observed on the secondary particle surface due to the limited lithium solubility in non-layered lattices. The extraction of both oxygen and lithium from the host material under elevated temperature could influence the chemistry and safety at the cell level via rearrangement of the electron and ion diffusion pathways, reduction of the Coulombic efficiency, and/or internal short circuit that could provoke a thermal runaway.

1. Introduction

Understanding the chemomechanical properties of battery electrodes can inform the design of battery materials and chemistry.[1,2] In particular, revealing the pathways of chemomechanical events in battery particles can provide mesoscopic insights into tailoring the local chemical inhomogeneity for enhancing battery stability. In battery materials, chemical heterogeneities can result from the purposely engineered compositional inhomogeneity[3,4] and/or different local lattice-structural ordering.[5] The heterogeneities are commonly amplified by prolonged electrochemical cycling,[4,6–8] which can cause multiscale buildup of mechanical strain,[9] morphological defects,[10] and mechanical degradation.[11,12] The development of mechanical strain and morphological defects affects the diffusion kinetics of the charge carriers (namely, Li ion and electron), leading to the state of charge (SOC) heterogeneity.[13] Such interdependent chemomechanical interplay collectively governs the structural and chemical evolution of the hierarchically architected battery electrodes and affects the cell-level performance.

The real-world battery operating conditions could introduce complex local chemical events that are undesired for sustaining battery cycle and safety. Commonly observed local chemical events include but are not limited to local overcharge/overdischarge,[14,15] oxygen release,[16] local structural transformation,[8,17] domain deactivation,[18] transition metal dissolution/precipitation,[6,8,19,20] and dendrite/whisker/protrusion growth.[21,22] The local regions that undergo these undesired chemical reactions may not account for much of the total mass or volume of the battery materials, but they can significantly impact the deliverable energy through impedance growth as well as undermine the safety characteristics of the battery cells through thermal runaway.[23,24]

Oxygen release from charged nickel-rich $LiNi_{1-x-y}Mn_xCo_yO_2$ (NMC) layered oxides, either through gas evolution or participating in electrolyte oxidation, has been reported under thermal abuse conditions[25,26] and aggressively charging to high voltages.[27] It is scientifically interesting and technologically relevant to investigate the thermally driven evolution of charged NMC cathode because the NMC material is generally less stable at the charged state. The oxygen loss is often accompanied by the lattice structural transformation from the layered structure to the rocksalt and/or spinel structures.[17,28] Such a structural transformation can lead to surface reconstruction at the primary particle level as well as the intergranular and intragranular cracks.[26,29] While the primary particle is the fundamental structural units of the active material, the secondary particle is regarded as important

[a] National Synchrotron Radiation Laboratory, University of Science and Technology of China, Hefei, Anhui 230027, China. E-mail: ychtian@ustc.edu.cn
[b] School of Materials Science and Engineering, Tianjin University, Tianjin 300072, China
[c] Stanford Synchrotron Radiation Lightsource, SLAC National Accelerator Laboratory, Menlo Park, California 94025, United States, E-mail: liuyijin@slac.stanford.edu
[d] Department of Chemistry, Virginia Tech, Blacksburg, Virginia 24061, United States, E-mail: fenglin@vt.edu
[e] Department of Geological Sciences, Stanford University, Stanford, California 94305, United States
[f] European Synchrotron Radiation Facility, Grenoble 38000, France
[g] Energy Storage & Distributed Resources Division, Lawrence Berkeley National Laboratory, Berkeley, California 94720, United States
[h] School of Mechanical Engineering, Purdue University, West Lafayette, Indiana 47906, United States

†Electronic Supplementary Information (ESI) available: [Material synthesis method and experimental details, soft XAS, SEM/EDS and TXM]. See DOI: 10.1039/x0xx00000x。

‡ C. Wei, Y. Zhang, and S.-J. Lee contributed equally to this work.

architectural building blocks for the battery electrode. Compared to the single-crystal primary particles, the secondary particles are populated with grain boundaries and morphological defects, e.g. cracks and voids. Therefore, the transmission x-ray microscopy (TXM), soft and hard x-ray absorption spectroscopy (XAS), scanning electron microscopy (SEM) and energy dispersive x-ray spectroscopy (EDS) to elucidate the thermally driven mesoscale chemomechanical

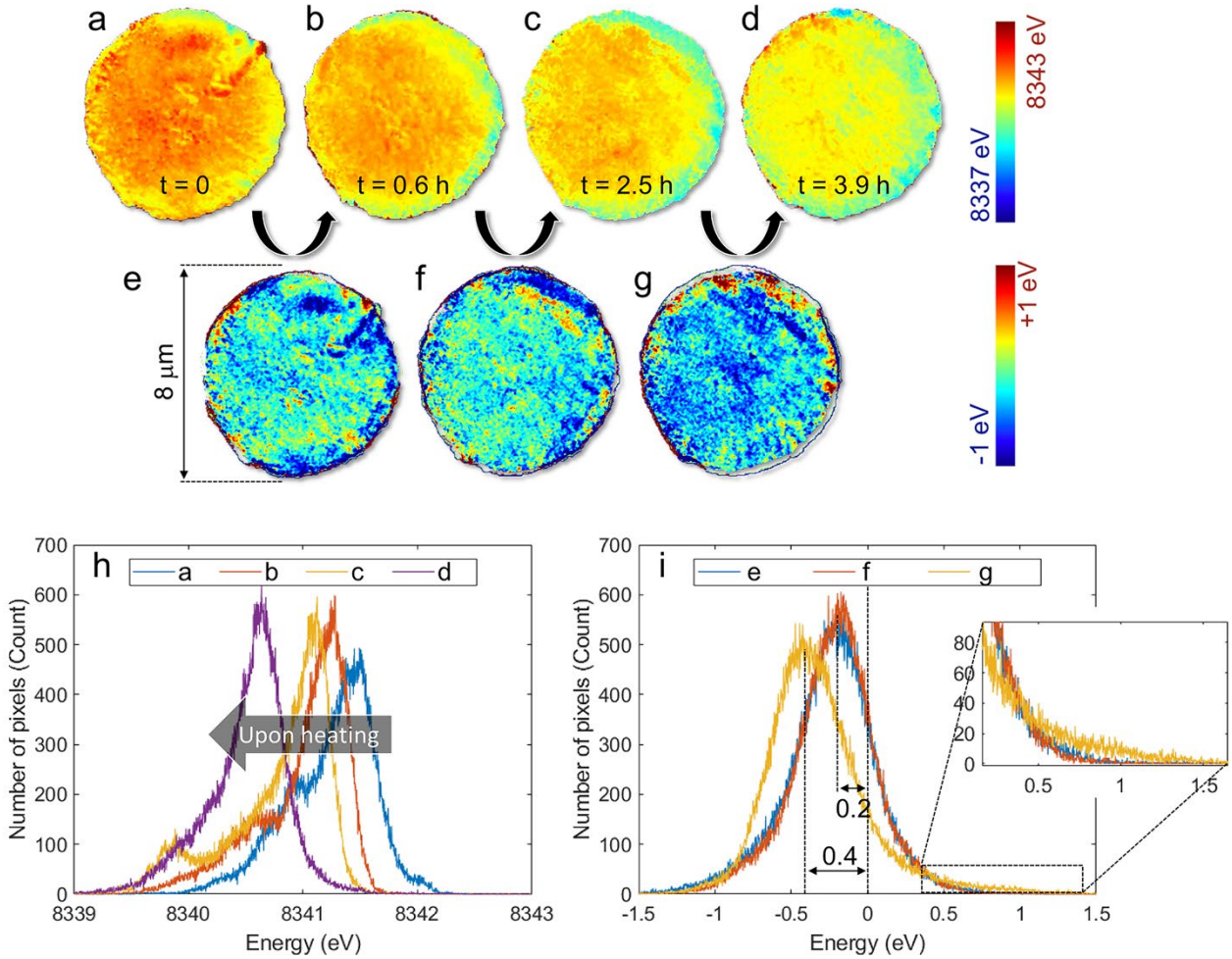

Fig. 1 Chemical evolution of a $Li_{0.5}Ni_{0.6}Mn_{0.2}Co_{0.2}O_2$ secondary particle recorded using full-field X ray spectro-microscopy under the thermal abuse condition (380 °C). Panels a-d show the evolution in the 2D distribution of Ni valence state (color coded to the corresponding color map with red and blue indicating more oxidized and more reduced domains, respectively) as the particle is exposed to high temperature for different amount of time. Panels e-g show the differential valence maps between a and b, b and c, c and d, respectively. Panel h shows that the probability distribution of the Ni's local valance state shifts toward lower energy upon heating. Panel i shows the probability distribution of the differential edge energy in panels e-g. The particle's diameter is about 8 microns.

structural and chemical complexity is further amplified at the mesoscale,[30] namely at the sub-secondary particle level. The knowledge of the mesoscale chemomechanical interplay is of fundamental and practical importance but is not yet well-established. Recently, we studied the thermally driven phase transformation in charged $LiNi_{0.4}Mn_{0.4}Co_{0.2}O_2$ (NMC442) secondary particle, which revealed that the propagation of the transformation front was governed by the local curvature of the valence isosurface.[25] This study provides the chemical basis for understanding the thermally driven mesoscale heterogeneous transformation in battery secondary particles. However, the mechanical aspect and, more importantly, the chemomechanical coupling at the mesoscale are still not well understood.

Herein, we study the mechanical and chemical responses of charged $Li_{0.5}Ni_{0.6}Mn_{0.2}Co_{0.2}O_2$ (NMC622) cathode material under thermal abuse conditions. We combined nanoscale coupling. We visualized and quantified the overall reduction of Ni as well as the internal Li redistribution at the early stage of the thermal abuse. The mechanical and morphological degradation upon heating is also observed in the nano-resolution x-ray tomographic (nano-tomography) data. At the later stage, on the particle surface we observe the growth of protrusions in forms of Li_2O, Li_2CO_3 or LiOH, the morphology and growing speed of which are influenced by the composition of the charged material. The thermally driven extraction of Li from the NMC cathode particle can distort and reconstruct the crystal structure of the host material. Depending on the composition and the properties (e.g. electronic and ionic conductivities) of the protrusion compound, this effect could reduce the Coulombic efficiency, shorten the battery life, and/or cause the capacity fade. Our work reveals the sophisticated thermally-driven chemomechanical coupling effect within NMC secondary particles and highlights the importance of mitigating the local

mechanical strain and chemical decomposition under thermal abuse conditions.

2. Results and discussion

Being exposed to thermal abuse conditions, the $Li_{0.5}Ni_{1-x-y}Mn_xCo_yO_2$ cathode material undergoes phase transformation from the R-3m layered structure to a mixed spinel/rocksalt structure.[25,26,31] Such a phase transformation is accompanied by the reduction of Ni cation and the release of lattice oxygen to oxidize the electrolyte solvent or release molecular oxygen.[16,27] In our earlier work, we investigated the local Ni valence states, which, to some extent, can serve as an indicator for quantifying the degree of oxygen release that occurs at the corresponding locations. We constructed 2D chemical isocontour and 3D chemical isosurface for more detailed investigation of the thermally driven dynamic evolution of the chemically delithiated $LiNi_{0.4}Mn_{0.4}Co_{0.2}O_2$ (NMC442).[25] In the present work, we turn to study electrochemically charged $Li_{0.5}Ni_{0.6}Mn_{0.2}Co_{0.2}O_2$ (NMC622) particle under elevated temperature up to 380°C for three reasons. First of all, the NMC compounds with higher Ni content is the trend of current research because the increment in Ni percentage improves the specific capacity.[32] Second, comparing to the samples prepared via chemical delithiation method,[28] the NMC particles that are cycled in real batteries can better reflect the active material's response to real-world battery electrochemistry because the electrolyte and the "inactive" components (carbon and binder) play an important role in affecting the local chemistry.[33] Third, although the chosen temperature at 380 °C seems to be higher than what one would expect under normal battery operating conditions, we point out here that a large variation of local current density could induce severe self-heating effect locally,[34] justifying our investigation at high temperature.

We carried out in operando 2D XANES mapping (Fig. S3) over the Ni K edge for a set of charged $Li_{0.5}Ni_{0.6}Mn_{0.2}Co_{0.2}O_2$ particles at 380 °C. The heating experiment was repeated in air and helium atmosphere, and similar phenomenon was observed. We investigate the cathode material from a coin cell that has gone through 6 electrochemical cycles (Fig. S1). The coin cell was then disassembled at the charged state (i.e., 4.5 V) in a glove box and the cathode was collected for further characterization. The charge distribution is heterogeneous in the pristine charged $Li_{0.5}Ni_{0.6}Mn_{0.2}Co_{0.2}O_2$ particle, which is consistent with our previous study.[33] Upon heating, the overall color of the maps changes from red (Fig. 1a) to orange (Fig. 1b-c) then to yellow (Fig. 1d), suggesting the continuous overall reduction of Ni cations upon heating. Our visual assessment and interpretation about the first order changes in the 2D Ni XANES maps are further confirmed by the evolution of the probability distribution of the Ni edge energy (Fig. 1h). As the particle is heated, the peak in Fig. 1h shifts towards the lower energy, in good agreement with the phenomenon observed in similar systems.[25]

A closer look at the in operando XANES maps, however, could provide more detailed information about the thermally driven reaction mechanisms. We show in Fig. 1e-g the differential valence maps between Fig. 1's panels: a and b, b and c, c and d, respectively. The local Ni oxidation process (as suggested by red-colored domains in Fig. 1e-g) takes place concurrently with the overall reduction of Ni. We show in Fig. 1i the probability distribution of the differential edge energy. The blue, red, and yellow curves in Fig. 1i are associated with Fig. 1e-g, respectively. While the peak positions are all at negative values, echoing the overall Ni reduction upon heating, positive components are clearly observed. The overall Ni reduction can be attributed to the well-known effect of oxygen release, however, to the best of our knowledge, the heating induced local Ni oxidation in this system has not been reported before. We attribute the local oxidation process to the thermally driven redistribution of Li ion in the host material. Additionally, in Fig. 1i, the blue and red curves show good symmetric shape in comparison to the yellow one. The probability distribution of the differential edge energy with good symmetry (blue and red curves in Fig. 1i) suggests that, at the early stage of the thermal treatment, the Li migration happens within the particle. This is because the degrees of Li-migration-induced local Ni reduction and oxidation are equivalent. Significant asymmetry is observed in the yellow curve in Fig. 1i, suggesting a more complicated reaction mechanism that involves charge transfer between the particle and the external system at the later stage of the thermal treatment, which will be revealed later in this paper.

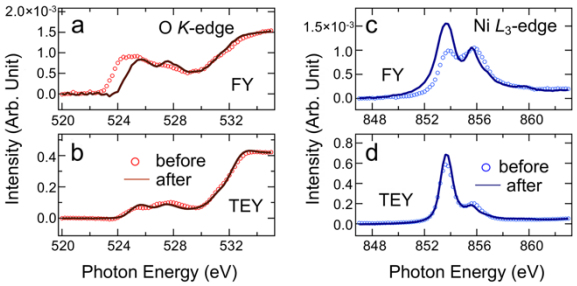

Fig. 2 Soft x-ray absorption spectroscopy (soft XAS) over O *K*-edge and Ni *L*-edge. Panels a and b are the soft XAS over the O *K*-edge in fluorescence yield (FY) mode and total electron yield (TEY) mode, respectively. Panels c and d are the soft XAS over the Ni *L*-edge in fluorescence yield (FY) mode and total electron yield (TEY) mode, respectively. The circles and the solid lines are from the $Li_{0.5}Ni_{0.6}Mn_{0.2}Co_{0.2}O_2$ sample before and after the thermal abuse, respectively.

Soft x-ray absorption spectroscopy was carried out to investigate the depth dependence of the thermally driven chemical evolution in this system. Fig. 2 shows the comparison of the O K-edge and Ni L3-edge spectra before and after the heat treatment in both the FY mode (Fig. 2a and 2c) and TEY mode (Fig. 2b and 2d). The TEY signal (probing depth at ~5 nm) doesn't seem to be much affected by the thermal treatment, possibly because of the fact that the electrochemical cycling has already induced lattice structural reconstruction on the particle surface from layered structure to spinel/rock salt structure.[26,28,35–37] In contrast, the FY signal (probing depth at ~50-100 nm) shows that the material was significantly reduced by the thermal treatment, suggesting that it is a bulk effect. The observed depth dependence appears to be similar over the O K-edge and the Ni L3-edge, highlighting the interplay between the redox reactions of the cation and the anion through Ni3d-O2p orbital hybridization.

It has been reported that the thermally driven chemical and mechanical processes in the NMC material interplay at fine length scales. At the primary particle level, the heating induced formation of the intergranular and intragranular cracks has been reported in our earlier publication.[2] Shortly after our work, similar phenomenon

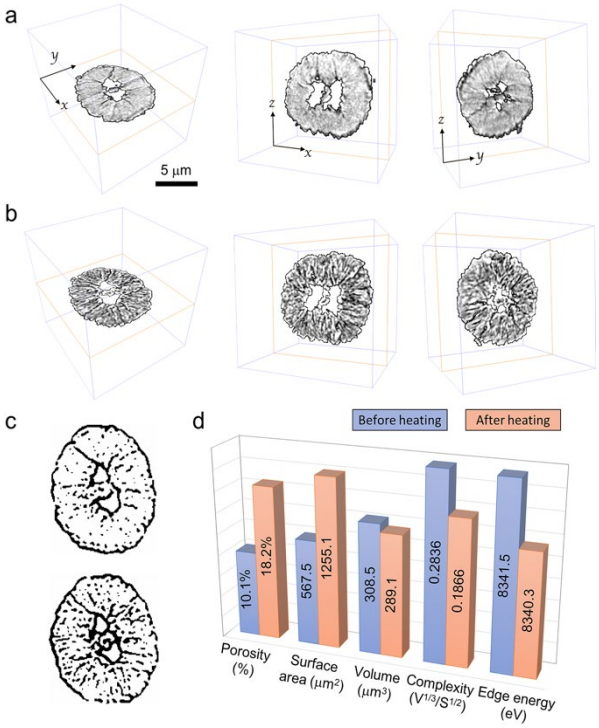

Fig. 3 Mechanical breakdown of a charged NMC622 secondary particle under thermal abuse conditions. Panel a shows the virtual slices through the center of the particle in different orientations. Panel b shows the corresponding slices after the particle was exposed to thermal abuse condition at 380 °C for ~4 hours. Panel c shows the segmentation of the cracks within the particle before (top) and after (bottom) the thermal treatment. Panel d shows the quantification of the particle's porosity, surface a Fig. S2) and averag process. The scale

cycling of the battery could have already induced morphological defects and SOC heterogeneity within and between the particles.[11,33,38,39]

For a more systematic evaluation of the mechanical breakdown of NMC secondary particles at the mesoscale, we employed in situ nano-tomography to investigate a selected NMC particle before and after it is exposed to thermal abuse conditions at 380 °C for ~ 4 hours. The virtual slices through the center of the particle in different orientations are shown in Fig. 3a (before thermal abuse) and b (after thermal abuse). The hole observed in the center of the particle exists in the pristine particles. Such as-made morphology has been seen in similar material systems.[6] Some electrochemical cycling induced cracks can be seen in Fig. 3a, in good agreement with our previous observations.[11] Much more radial cracks are observed in the same particle after the thermal treatment, as highlighted by the segmentation of the cracks (Fig. 3c) based on an edge detection algorithm.[40] We further quantified the porosity, the surface area, the total volume, the morphological complexity (see Fig. S2), and the averaged edge energy of this particle before and after the thermal abuse (see Fig. 3d). Both the porosity and crack surface area are increased dramatically by nearly a factor of 2, making the morphological complexity parameter (ε=V1/3/S1/2; the smaller ε, the higher degree of morphological complexity[6]) change from 0.2836 to 0.1866. The change in ε confirms the significant development of the morphological defects and, thus, the morphological complexity upon heating. Our observations confirm that the mechanical and chemical characteristics of the NMC particle are highly correlated at the mesoscale. The battery electrode's self-heating effect (in particular under fast charging conditions) could, therefore, lead to rearrangement of the mesoscale current distribution through mechanical disintegration of the secondary particles. The altered current density distribution could effectively redistribute the heat

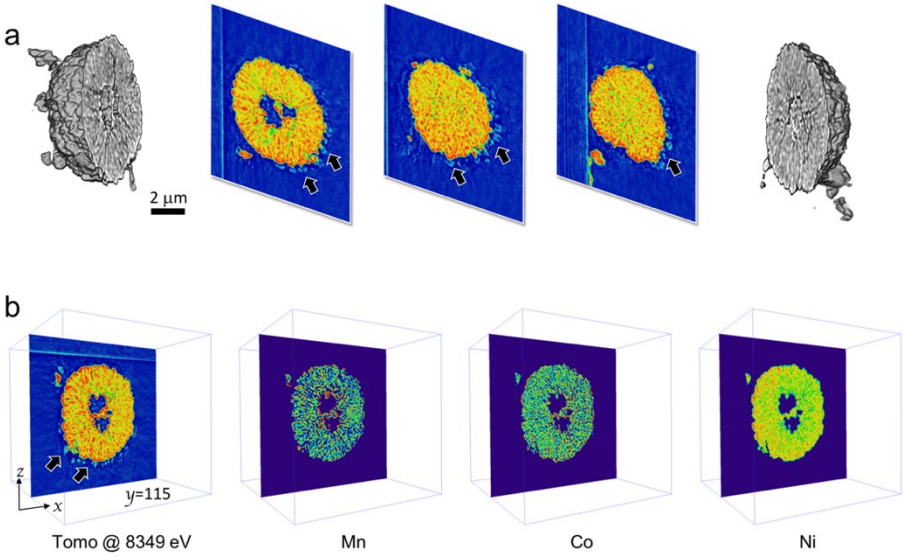

Fig. 4 Three-dimensional mapping of the transition metal elements within the thermally abused $Li_{0.5}Ni_{0.6}Mn_{0.2}Co_{0.2}O_2$ particle. Panel a is the single energy (8349 eV) nano-tomographic data: the 3D rendering and three virtual slices through different depth of the particle in the xz plane. Panel b are the virtual slices through the center of the particle in xz plane. The left image in panel b is the single energy tomographic data while the other images in panel b are the corresponding elemental maps of Mn, Co, and Ni, respectively, over the same plane. The low contrast protrusions on the particle surface (black arrows) do not appear in the maps of the transition metals. The scale bar in column a is 2 microns.

has been reported by other groups,[29] in good agreement with our conclusions. As a result, one could project the nanoscale observation to the mesoscale and could speculate that thermal abuse conditions might cause disintegration of the secondary particle. However, it is more complicated at the mesoscale, because the electrochemical load, which, in turn, will trigger more complicated thermally driven reactions in the system.

In addition to the mesoscale mechanical breakdown, shown in the nano-tomographic data, we also observe some nearly transparent features on the particle surface after the thermal treatment. As shown in the virtual slices through different depth on the particle (Fig. 4a), the protrusions (see black arrows in Fig. 4a) on the particle surface are of much smaller absorption coefficient at 8349 eV comparing to that of the particle. We further conducted the nano-tomography at 6 different x-ray energies, above and below the absorption K-edges of Mn, Co, and Ni, respectively (Fig. S4). As shown in Fig. 4b, the protrusions on the particle surface are canceled out when calculating the differential nano-tomographic data above and below the absorption edges for the extraction of the maps specific to the corresponding transition metal elements. To further support this argument, scanning electron microscopy (SEM) and energy dispersive spectroscopy (EDS) are employed to reveal the composition of the observed protrusions (Fig. 5). The local EDS result (Fig. 5b) confirms that the protrusions over the particle surface is free of transition metals, in good agreement with the TXM data shown in Fig. 4.

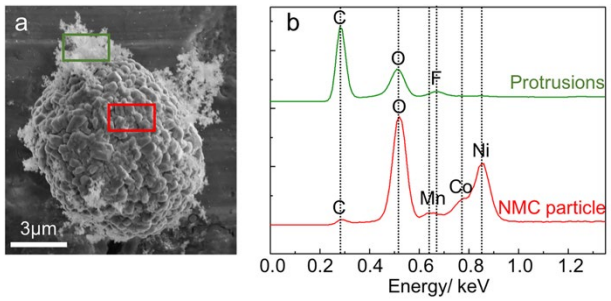

Fig. 5 Scanning electron microscopy (panel a) and energy dispersive x-ray spectroscopy (panel b) of an NMC particle that has gone through the thermally abuse conditions (380 °C for ~4 hours).

Similarly, the thermally induced Li compound protrusions are also observed in an in operando x-ray imaging experiment of hollow

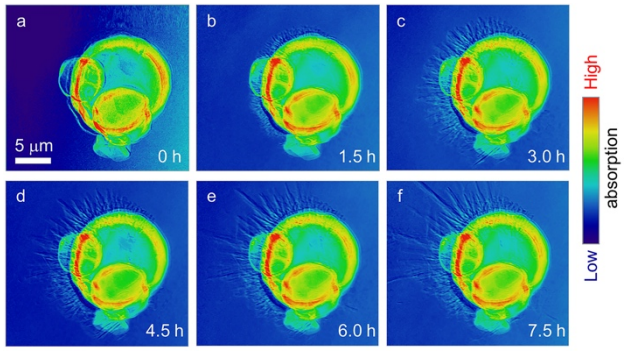

Fig. 6 Thermally driven Li compound protrusions growth on the surface of hollow spherical $LiNi_{0.4}Mn_{0.4}Co_{0.2}O_2$ particles, which are prepared by spray pyrolysis method. Panels a-f are *in situ* monitoring of the particle with interval of 1.5 hours. The scale bar in panel a is 5 microns.

spherical $LiNi_{0.4}Mn_{0.4}Co_{0.2}O_2$ (NMC442) particles (Fig. 6) prepared by a spray pyrolysis method.[3,41] In this case, the protrusions appear to be whiskers growing on the particle's surface. A thin layer (~1 μm) of the whisker is already observed after the particle is heated for only 1.5 hours. It continues to develop in a very inhomogeneous manner. It is interesting that the morphology of the Li compound protrusions is very different depending on the composition of the starting material. The Li compound protrusions with different morphology could have different impacts. The protrusion in the form of whiskers could potentially facilitate the direct interaction among different particles that are spatially separated by tens of microns, whereas the first direct impacts of the lump-shaped protrusions are more likely to be confined locally.

The thermally driven development of Li compound protrusions on charged NMC cathode particle surface is an unanticipated phenomenon. While the metallic Li dendrite growth is a known issue for battery operation, it often emanates out of the Li metal anode. High local current density induced self-heating effect has been reported to favor the suppression of Li dendrite growth in Li-sulfur batteries by facilitating extensive surface migration of Li metal.[34] The protrusions observed in our experiment survives the temperature at up to 380 °C, which is significantly higher than the melting point of Li metal at ~180 °C. As a result, we rule out the metallic Li as a possibility and conjecture that the protrusions on the particle surface is likely in the form of Li_2O, Li_2CO_3 or LiOH. The thermally driven development of the Li protrusions causes irreversible consumption of useful lithium in the battery. Depending on the composition and the properties (e.g. electronic and ionic conductivities) of the protrusion compound, this effect could affect the cathode-electrolyte interphase and cause the rearrangement of the electron and ion diffusion pathways and, subsequently, reduce the Coulombic efficiency, shorten the battery life, and/or cause the capacity fade.

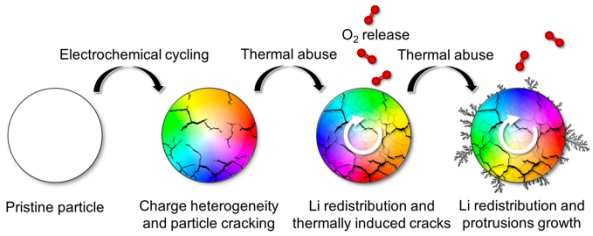

Fig. 7 Schematics of the thermally driven mesoscale chemomechanical interplay in charged NMC particles. While the electrochemical cycling induces the initial SOC heterogeneity and particle cracking, thermal abuse conditions cause redistribution of Li within the particle and lead to additional mechanical breakdown at mesoscale, which is accompanied by oxygen release. Further heating could lead to Li compound protrusions on the particle surface.

3. Conclusions

While lithium ion batteries are often designed to be operated within a mild temperature window, extreme temperature spikes could occur due to many reasons. In particular, at the nano to meso scales, the structural and chemical complexity could lead to very large local current, which could induce severe local self-heating effect.[34] Under thermal abuse conditions, the charged battery electrode material undergoes sophisticated reactions that involve chemomechanical interplay at many different length scales. In this work, we systematically investigate the response of the $Li_{0.5}Ni_{0.6}Mn_{0.2}Co_{0.2}O_2$ cathode particles to the elevated temperature up to 380 °C. Synchrotron based characterization techniques[42] including x-ray microscopy, hard and soft x-ray absorption spectroscopy are combined with SEM-EDX to elucidate the thermally driven reaction mechanism at the mesoscale, which is illustrated in Fig. 7. While the morphological defects and SOC heterogeneity were already induced

by the electrochemical cycling prior to the thermal abuse, elevated environmental temperature causes oxygen release, which is associated with more crack formation at both the nanoscale and mesoscale. In the early stage of the heating process, we observed thermally driven redistribution of Li within the particle. Further thermal abuse will lead to extraction of Li from the host material, likely in the forms of Li_2O, Li_2CO_3 or LiOH. The morphology and growing speed of the Li protrusions are heavily dependent on the composition of the host material. This phenomenon was observed in the heating experiments in the atmosphere of both helium and air. Our study suggests that the phase transformation under thermal abuse conditions is a collective process of losing lithium and oxygen from the lattice. Depending on the chemical and physical properties of the Li-based protrusions, this effect could influence the cell level chemistry via rearranging the electron and ion diffusion pathways and, subsequently, reduce the Coulombic efficiency, shorten the battery life, and/or cause the capacity fade. The irreversible consumption of the Li inventory in the cell will also negatively impact the overall functionality of the system.

Author Contributions

Y. Liu and F. Lin designed the project. C. Wei, Y. Zhang, S.-J. Lee, L. Mu, J. Liu, C. Wang, J.-S. Lee, F. Lin and Y. Liu performed the experiments. C. Wei, Y. Zhang, S.-J. Lee, J.-S. Lee, F. Lin, and Y. Liu analyzed the data. M. Doeff, K. Zhao, P. Pianetta, D. Nordlund, X.-W. Du, Y. Yang and Y. Tian contributed to the interpretation of the experimental data. C. Wei, Y. Zhang, S.-J. Lee, F. Lin and Y. Liu prepared the manuscript with critical inputs from all the authors. C. Wei, Y. Zhang, and S.-J. Lee contributed equally to this work.

Conflicts of interest

There are no conflicts to declare.

Acknowledgements

The work at Virginia Tech was supported by the Department of Chemistry Startup at Virginia Tech. Use of the Stanford Synchrotron Radiation Lightsource, SLAC National Accelerator Laboratory, is supported by the U.S. Department of Energy, Office of Science, Office of Basic Energy Sciences under Contract No. DE-AC02-76SF00515. Part of this work was performed at the Stanford Nano Shared Facilities (SNSF), supported by the National Science Foundation under award ECCS-1542152. F.L. and K.Z. acknowledge support from the National Science Foundation under Grants No. DMR-1832613 and DMR-1832707, respectively. The NMC electrodes were produced at the U.S. Department of Energy's (DOE) CAMP (Cell Analysis, Modeling and Prototyping) Facility, Argonne National Laboratory. The CAMP Facility is fully supported by the DOE Vehicle Technologies Program (VTP) within the core funding of the Applied Battery Research (ABR) for Transportation Program. The engineering support from D. Van Campen, D. Day and V. Borzenets for the TXM experiment at beamline 6-2C of SSRL is gratefully acknowledged. The authors also thank Ryan Davis and Matthew Latimer for their support at beamlines 4-1 and 2-2 of SSRL. C. Wei and Y. Zhang were supported by the China Scholarship Council for their study at the SLAC National Accelerator Laboratory.

Reference

1 Z. Xu, M. M. Rahman, L. Mu, Y. Liu and F. Lin, Journal of Materials Chemistry A, in press .
2 K. Zhao and Y. Cui, Extreme Mechanics Letters, 2016, 9, 347–352.
3 F. Lin, D. Nordlund, Y. Li, M. K. Quan, L. Cheng, T.-C. Weng, Y. Liu, H. L. Xin and M. M. Doeff, Nature Energy, 2016, 1, 15004.
4 M. M. Rahman, Y. Xu, H. Cheng, Q. Shi, R. Kou, L. Mu, Q. Liu, S. Xia, X. Xiao, C.-J. Sun, D. Sokaras, D. Nordlund, J.-C. Zheng, Y. Liu and F. Lin, Energy & Environmental Science, 2018, DOI:10.1039/C8EE00309B.
5 W. H. Kan, B. Deng, Y. Xu, A. K. Shukla, T. Bo, S. Zhang, J. Liu, P. Pianetta, B.-T. Wang, Y. Liu and G. Chen, Chem, 2018, 4, 1-16.
6 F. Yang, Y. Liu, S. K. Martha, Z. Wu, J. C. Andrews, G. E. Ice, P. Pianetta and J. Nanda, Nano Letters, 2014, 14, 4334–4341.
7 Y. Xu, E. Hu, K. Zhang, X. Wang, V. Borzenets, Z. Sun, P. Pianetta, X. Yu, Y. Liu, X.-Q. Yang and H. Li, ACS Energy Letters, 2017, 2, 1240–1245.
8 J. D. Steiner, L. Mu, J. Walsh, M. M. Rahman, B. Zydlewski, F. M. Michel, H. L. Xin, D. Nordlund and F. Lin, ACS Applied Materials & Interfaces, 2018, 10, 23842–23850.
9 A. Singer, M. Zhang, S. Hy, D. Cela, C. Fang, T. A. Wynn, B. Qiu, Y. Xia, Z. Liu, A. Ulvestad, N. Hua, J. Wingert, H. Liu, M. Sprung, A. V. Zozulya, E. Maxey, R. Harder, Y. S. Meng and O. G. Shpyrko, Nature Energy, 2018, 3, 641–647.
10 R. Xu, L. S. de Vasconcelos, J. Shi, J. Li and K. Zhao, Experimental Mechanics, 2018, 58, 549–559.
11 S. Xia, L. Mu, Z. Xu, J. Wang, C. Wei, L. Liu, P. Pianetta, K. Zhao, X. Yu, F. Lin and Y. Liu, Nano energy, 2018, 53, 753-762.
12 P. Yan, J. Zheng, M. Gu, J. Xiao, J.-G. Zhang and C.-M. Wang, Nature Communications, 2017, 8, 14101.
13 Y. Xu, E. Hu, F. Yang, J. Corbett, Z. Sun, Y. Lyu, X. Yu, Y. Liu, X.-Q. Yang and H. Li, Nano Energy, 2016, 28, 164–171.
14 T. Ohsaki, T. Kishi, T. Kuboki, N. Takami, N. Shimura, Y. Sato, M. Sekino and A. Satoh, Journal of Power Sources, 2005, 146, 97–100.
15 J. Nelson Weker, A. M. Wise, K. Lim, B. Shyam and M. F. Toney, Electrochimica Acta, 2017, 247, 977–982.
16 E. Hu, S.-M. Bak, Y. Liu, J. Liu, X. Yu, Y.-N. Zhou, J. Zhou, P. Khalifah, K. Ariyoshi, K.-W. Nam and X.-Q. Yang, Advanced Energy Materials, 2016, 6, 1501662.
17 F. Lin, I. M. Markus, D. Nordlund, T.-C. Weng, M. D. Asta, H. L. Xin and M. M. Doeff, Nature Communications, 2014, 3529.
18 K. Zhang, F. Ren, X. Wang, E. Hu, Y. Xu, X.-Q. Yang, H. Li, L. Chen, P. Pianetta, A. Mehta, X. Yu and Y. Liu, Nano Letters, 2017, 17, 7782–7788.
19 E. Billy, M. Joulié, R. Laucournet, A. Boulineau, E. De Vito and D. Meyer, ACS Applied Materials & Interfaces, 2018, 10, 16424–16435.
20 Y. Li, Y. Xu, Z. Wang, Y. Bai, K. Zhang, R. Dong, Y. Gao, Q. Ni, F. Wu, Y. Liu and C. Wu, Advanced Energy Materials, 2018, DOI:10.1002/aenm.201800927.
21 L. A. Selis and J. M. Seminario, RSC Advances, 2018, 8, 5255–5267.
22 X. Wang, W. Zeng, L. Hong, W. Xu, H. Yang, F. Wang, H. Duan, M. Tang and H. Jiang, Nature Energy, 2018, 3, 227–235.
23 A. W. Golubkov, D. Fuchs, J. Wagner, H. Wiltsche, C. Stangl, G. Fauler, G. Voitic, A. Thaler and V. Hacker, RSC Adv., 2014, 4, 3633–3642.

24 D. P. Finegan, M. Scheel, J. B. Robinson, B. Tjaden, I. Hunt, T. J. Mason, J. Millichamp, M. Di Michiel, G. J. Offer, G. Hinds, D. J. L. Brett and P. R. Shearing, Nature Communications, 2015, 6, 6924.
25 L. Mu, Q. Yuan, C. Tian, C. Wei, K. Zhang, J. Liu, P. Pianetta, M. M. Doeff, Y. Liu and F. Lin, Nature Communications, 2018, 9, 2810.
26 L. Mu, R. Lin, R. Xu, L. Han, S. Xia, D. Sokaras, J. D. Steiner, T.-C. Weng, D. Nordlund, M. M. Doeff, Y. Liu, K. Zhao, H. L. Xin and F. Lin, Nano Letters, 2018, 18, 3241–3249.
27 R. Jung, M. Metzger, F. Maglia, C. Stinner and H. A. Gasteiger, Journal of The Electrochemical Society, 2017, 164, A1361–A1377.
28 F. Lin, D. Nordlund, I. M. Markus, T.-C. Weng, H. L. Xin and M. M. Doeff, Energy & Environmental Science, 2014, 7, 3077.
29 P. Yan, J. Zheng, T. Chen, L. Luo, Y. Jiang, K. Wang, M. Sui, J.-G. Zhang, S. Zhang and C. Wang, Nature Communications, 2018, 9, 2437.
30 C. Wei, S. Xia, H. Huang, Y. Mao, P. Pianetta and Y. Liu, Accounts of Chemical Research, 2018, DOI:10.1021/acs.accounts.8b00123.
31 F. Lin, I. M. Markus, M. M. Doeff and H. L. Xin, Scientific Reports, 2015, 4, 5694.
32 J. Xu, F. Lin, M. M. Doeff and W. Tong, Journal of Materials Chemistry A, 2017, 5, 874–901.
33 C. Tian, Y. Xu, D. Nordlund, F. Lin, J. Liu, Z. Sun, Y. Liu and M. Doeff, Joule, 2018, 2, 464–477.
34 L. Li, S. Basu, Y. Wang, Z. Chen, P. Hundekar, B. Wang, J. Shi, Y. Shi, S. Narayanan and N. Koratkar, Science, 2018, 359, 1513–1516.
35 F. Lin, D. Nordlund, T.-C. Weng, Y. Zhu, C. Ban, R. M. Richards and H. L. Xin, Nature Communications, 2014, 5, 3358.
36 F. Lin, D. Nordlund, T. Pan, I. M. Markus, T.-C. Weng, H. L. Xin and M. M. Doeff, J. Mater. Chem. A, 2014, 2, 19833–19840.
37 S.-K. Jung, H. Gwon, J. Hong, K.-Y. Park, D.-H. Seo, H. Kim, J. Hyun, W. Yang and K. Kang, Advanced Energy Materials, 2014, 4, 1300787.
38 J. Wang, Y. Karen Chen-Wiegart, C. Eng, Q. Shen and J. Wang, Nature Communications, 2016, 7, 12372.
39 S. Kuppan, Y. Xu, Y. Liu and G. Chen, Nature Communications, 2017, 8, 14309.
40 D. Vikram Mutneja, Journal of Electrical & Electronic Systems, 2015, 4, 1000150.
41 J. B. Mooney and S. B. Radding, Annual Review of Materials Science, 1982, 12, 81–101.
42 F. Lin, Y. Liu, X. Yu, L. Cheng, A. Singer, O. G. Shpyrko, H. L. Xin, N. Tamura, C. Tian, T.-C. Weng, X.-Q. Yang, Y. S. Meng, D. Nordlund, W. Yang and M. M. Doeff, Chemical Reviews, 2017, 117, 13123–13186.